Exceptional Points as Manifestations of Analyticity Breakdown in the 't Hooft Model

Kejun Liu[1, 2, *]

[1] *Institute of Functional Nano & Soft Materials (FUNSOM), Soochow University, Suzhou 215123, China*
[2] *School of Physical Science and Technology, Soochow University, Suzhou 215006, China*

We use the exactly-solvable 't Hooft model of 1+1D large-N_c QCD as a rigorous laboratory for the breakdown of analyticity of a causal response function, the meson two-point function. A PT-symmetric deformation $i\gamma(x-1/2)$ of the light-cone meson operator, the analogue of an imaginary chemical potential, drives the lowest two mesons to an exceptional point (EP) at γ_c. Recasting the resolvent as a Jacobi continued fraction yields γ_c in closed form: $2\pi g^2 N_c$ at the two-pole level, converging to $7.966\, g^2 N_c$ by depth five—an analytic, not numerical, threshold. The square-root exponent $\nu = 1/2$ is fixed by the 2×2 Jordan form and confirmed by finite-size scaling to $N = 1999$. The breakdown has an unambiguous time-domain signature: the propagator norm $\|e^{-iHt}\|$ is bounded for $\gamma < \gamma_c$, grows *linearly* at γ_c (the Jordan secular law), and exponentially beyond—observable, since the deformed operator is a non-Hermitian Wannier-Stark ladder, in photonic and topolectrical analogues. The threshold is locked to confinement, $\gamma_c \propto g^2 N_c$, and recurs as a uniform EP cascade; a second, non-reciprocal deformation yields an exactly-exponential non-Hermitian skin effect. This is the first analytically-controlled instance of exceptional-point analyticity breakdown in a confining gauge theory.

I. INTRODUCTION

The meson propagator of a confining gauge theory is a causal response function. In the 't Hooft model—1+1D SU(N_c) QCD at large N_c [1, 2]—it is the two-point function $G(z) = \langle\phi_0|(z-V)^{-1}|\phi_0\rangle$ of the light-cone meson operator V (defined in §2), analytic in the upper-half plane of the squared mass z, with poles on the real axis at $M_n^2 = \pi g^2 N_c\, n$ forming the physical spectrum. Causality fixes this analytic structure: G is a Herglotz/Nevanlinna function and obeys Kramers-Kronig (KK) relations [3, 4]. A sharp question—shared by open quantum systems [5], non-Hermitian photonics [6], and finite-density field theory [7, 8]—is *where and how this analyticity fails* once the underlying operator is rendered non-Hermitian. Exceptional points (EPs)—non-Hermitian degeneracies where eigenvalues and eigenvectors coalesce [9, 10], a cornerstone of PT-symmetric and non-Hermitian physics [6] following Bender and Boettcher [11]—are the natural mechanism: an EP is a branch point, and crossing it forces a response function onto a second Riemann sheet—a causality breaking that carries a topological (Blaschke-winding) charge in non-Hermitian dimers [12]. What has been lacking is an exactly-solvable, non-perturbative field theory in which this breakdown can be located and characterised in closed form.

We provide one. The 't Hooft equation reduces to a single integral operator with the analytically known, equidistant spectrum $M_n^2 = \pi g^2 N_c\, n$ quoted above. We deform it by a PT-symmetric term $i\gamma(x-1/2)$, the momentum-fraction analogue of an imaginary chemical potential [7, 8], and ask at what coupling the meson resolvent loses analyticity. Three results follow, each addressing a facet of the breakdown:

Where: γ_c is the analyticity radius of the resolvent and, because the deformed operator is tridiagonal, the root of a Jacobi continued fraction—$2\pi g^2 N_c$ at the two-pole truncation, converging to $7.966\, g^2 N_c$ by depth five. The location is analytic, not a numerical black box.

How: the singularity is a square-root branch point, exponent $\nu = 1/2$ fixed by the 2×2 Jordan normal form and confirmed by finite-size scaling to $N = 1999$.

What is observed: the breakdown has a sharp dynamical fingerprint—the propagator norm grows *linearly* in time exactly at γ_c (the Jordan secular law), between bounded ($\gamma < \gamma_c$) and exponential ($\gamma > \gamma_c$) regimes—measurable in non-Hermitian lattice analogues.

The threshold is moreover locked to confinement, $\gamma_c \propto g^2 N_c$, recurring as a uniform EP cascade, and a second, non-reciprocal kernel realises the non-Hermitian skin effect (NHSE) in closed form. Prior non-Hermitian gauge theory builds intrinsically non-Hermitian QCD extensions perturbatively [13–15] or studies PT transitions in effective models [16, 17]; we instead deform an exactly-solvable confining theory, which renders the analyticity breakdown tractable in closed form.

II. SETUP: MESON RESOLVENT AND WEIGHTED HERMITICITY

In light-cone gauge $A^+ = 0$, the 't Hooft equation is [1]

$$M^2\phi(x) = \mu^2\, P\!\int_0^1 \frac{\phi(y)}{(x-y)^2}\,dy + \Big(\frac{m_1^2}{x} + \frac{m_2^2}{1-x}\Big)\phi(x),$$
$$\mu^2 = \frac{g^2 N_c}{\pi}, \tag{1}$$

* kjliu@suda.edu.cn

with $\phi(0)=\phi(1)=0$ and P the Hadamard finite part (the second-order kernel is not principal-value integrable; regularisation, domain $D(V)$ of endpoint-vanishing $\phi\sim\sqrt{x(1-x)}$, and deficiency indices in the Supplemental Material). In the chiral limit $m_1=m_2=0$, writing $(V\phi)(x)=\mu^2\,P\!\int_0^1\phi(y)/(x-y)^2\,dy$, the central object is the meson resolvent,

$$G(z;\gamma)=\langle\phi_0|(z-V(\gamma))^{-1}|\phi_0\rangle,\quad V(\gamma)=V+i\gamma(x-\tfrac{1}{2}). \tag{2}$$

a response function whose analytic structure in z (poles at the M_n^2) and in the coupling γ encodes the spectral data.

At $\gamma=0$, V is non-Hermitian in flat $L^2[0,1]$ but Hermitian with respect to the weighted inner product $\langle\phi,\psi\rangle_J=\int_0^1\phi\bar{\psi}\,[x(1-x)]^{-1/2}dx$. Since $J=[x(1-x)]^{-1/2}>0$ the resulting space is a genuine (positive-definite) Hilbert space, not a Krein space; the change of variable $x=\sin^2(\theta/2)$ maps it isometrically to $L^2(0,\pi)$, where V is diagonalised by $\sin n\theta$, giving the Gegenbauer eigenfunctions and $M_n^2=\pi g^2N_c\,n$ [18, 19]. The operator is essentially self-adjoint on this eigenbasis, which guarantees a real spectrum—a property distinct from indefinite-metric pseudo-Hermiticity [20]. Positivity $M_n^2>0$ is the separate, model-specific content of the exact solution. In this basis $G(z;0)=\sum_n|c_n|^2/(z-M_n^2)$ is a Herglotz function—a hallmark of causal response—and the deformation $i\gamma(x-1/2)=-\frac{i\gamma}{2}\cos\theta$ is tridiagonal, $\langle\sin m\theta|\cos\theta|\sin n\theta\rangle=\frac{1}{2}(\delta_{m,n+1}+\delta_{m,n-1})$.

III. THE EXCEPTIONAL POINT AS A BRANCH POINT OF $G(z;\gamma)$

As γ increases, the lowest two poles of G, at $M_1^2(\gamma)$ and $M_2^2(\gamma)$, approach and at $\gamma=\gamma_c$ coalesce into a single defective eigenvalue: the eigenvectors become parallel (phase rigidity $r_1\to0$~[5, 21]) and G develops, in the variable γ, a square-root branch point. For $\gamma>\gamma_c$ the two masses form a complex-conjugate pair,

$$M_{1,2}^2(\gamma)=E_*\pm iC\sqrt{\gamma-\gamma_c}+\mathcal{O}(\gamma-\gamma_c). \tag{3}$$

The exponent is not a fitting parameter: at γ_c the 2×2 invariant block is $E_*I+\mathcal{N}$ with $\mathcal{N}^2=0$, $\mathcal{N}\neq0$, and analytic perturbation of a defective eigenvalue carrying a size-2 Jordan block has a Puiseux series with leading term $\pm\sqrt{\gamma-\gamma_c}$ [10, 22]. Thus $\nu=1/2$ is fixed by the Jordan normal form; the role of the numerics [Fig. 1(a,b)] is to confirm true order-2 coalescence and to locate γ_c.

The threshold from the J-fraction. Because $V(\gamma)$ is tridiagonal (a Jacobi matrix), the resolvent (2) is a Jacobi continued fraction, with $a_n=\pi g^2N_c\,n$ and $b_n=-i\gamma/4$,

$$G(z;\gamma)=\cfrac{1}{z-a_1-\cfrac{b_1^2}{z-a_2-\cfrac{b_2^2}{z-a_3-\cdots}}}. \tag{4}$$

Its off-diagonals are imaginary, $b_n^2=-\gamma^2/16<0$, so (4) is a *complex* Jacobi continued fraction [23]—the analytic continuation in γ of the $\gamma=0$ Herglotz fraction of §2—whose poles leave the real axis above γ_c. The EP is where the two lowest poles collide; truncating at depth K and solving for the coalescence gives a *convergent sequence of approximants*, the two-pole convergent ($K=2$) being the closed form

$$\gamma_c^{(K=2)}=2\pi\,g^2N_c\;(\approx6.283\,g^2N_c),$$

and deeper convergents approach the limit rapidly [Fig. 2(a)],

$$\gamma_c(K)/g^2N_c:\quad 6.283\xrightarrow{K=3}8.886\xrightarrow{K=4}7.948\xrightarrow{K\geq5}\boxed{7.966}, \tag{5}$$

saturating to four digits by depth five and stable through $K=256$; the EP is controlled by the lowest five rungs, the $\sim27\%$ shift from 2π being the contribution of the higher mesons, not a discretisation artefact. The non-monotone approach (the $K=3$ convergent overshoots) is a finite-truncation artefact: an odd symmetric truncation pins its central level, giving a spurious third-order coalescence at $K=3$, while even and larger truncations recover the physical order-2 EP (closed-form factorisation in SM S2.3).

Finite-size scaling fixes the exponent. With the γ-window centred on γ_c, $\nu(N)$ descends from 0.5045 ($N=199$) to 0.5001 ($N=1999$), extrapolating in $1/N$ to $\nu_\infty=0.4993$—within 7×10^{-4} of 1/2, and to 0.5000 under a quadratic $1/N^2$ fit (the residual is finite-N curvature; $\nu=1/2$ is fixed by the Jordan form regardless) [Fig. 1(a), Table S1]. The fine γ-mesh confirms the mechanism [Fig. 1(b)]: the spectrum is real to within 10^{-11} below γ_c, and $|\mathrm{Im}\,M^2|\propto(\gamma-\gamma_c)^{0.504}$ above it.

IV. DYNAMICAL FINGERPRINT OF THE BREAKDOWN

The branch point has a direct time-domain signature, free of the phase-convention ambiguities of non-Hermitian inner products: the operator norm of the propagator. For each fixed $\gamma<\gamma_c$ the spectrum is real and $V(\gamma)$ is diagonalisable, so the spectral (operator) norm $\|e^{-iV(\gamma)t}\|$ is bounded in t by the eigenvector condition number $\kappa(S)$—a bound that is not uniform: $\kappa(S)\to\infty$ as $\gamma\to\gamma_c^-$, the pre-critical signature

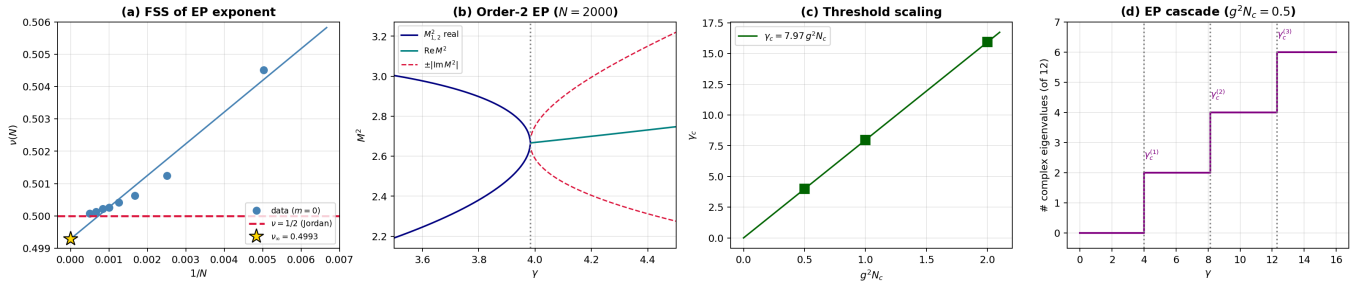

FIG. 1. (a) FSS of the EP exponent $\nu(N)$ ($m = 0$, identical for $g^2N_c = 0.5, 1, 2$); $\nu_\infty = 0.4993$ vs the analytic $1/2$ (dashed). (b) Eigenvalues near the EP (fine γ-mesh, $N = 2000$): two real branches coalesce at γ_c and split into a $\pm|\mathrm{Im}\, M^2|$ square-root envelope. (c) The threshold scales linearly with the coupling, $\gamma_c = 7.966\, g^2N_c$. (d) Beyond γ_c, the complex-eigenvalue count rises in steps of two at $\gamma_c^{(k)} \simeq k\,\gamma_c^{(1)}$: a uniform EP cascade locked to the equidistant spectrum.

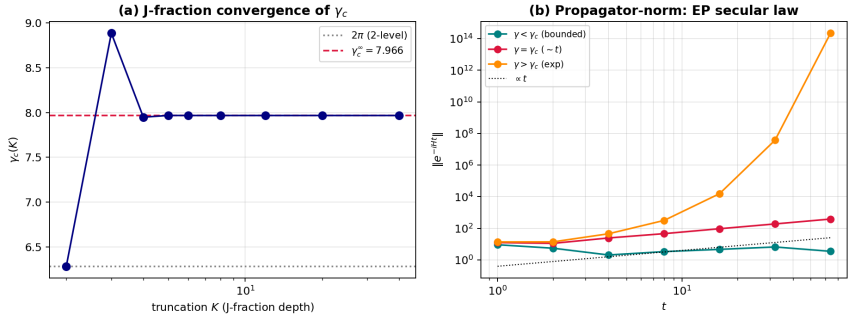

FIG. 2. (a) The threshold $\gamma_c(K)$ from the J-fraction (4): exactly 2π at the two-pole level, converging to 7.966 by depth $K = 5$ (stable to $K = 256$). (b) Propagator norm $\|e^{-iVt}\|$: bounded for $\gamma < \gamma_c$, linear in t at γ_c (parallel to the dotted $\propto t$), exponential for $\gamma > \gamma_c$ — the Jordan secular law.

of the approaching defect. Exactly at γ_c, exponentiating the defective 2×2 Jordan block $E_*I + \mathcal{N}$ yields $e^{-i(E_*I+\mathcal{N})t} = e^{-iE_*t}(I - i\mathcal{N}t)$, so

$$\left\|e^{-iV(\gamma_c)t}\right\| \;\sim\; t \qquad \text{(secular, Jordan)}, \tag{6}$$

a *linear* growth, while for $\gamma > \gamma_c$ the complex pair leads to exponential growth at rate $\max \mathrm{Im}\, M^2 \propto \sqrt{\gamma - \gamma_c}$. We confirm this three-regime law numerically [Fig. 2(b)]: a log-log fit of $\|e^{-iVt}\|$ ($t \geq 4$) gives a sub-linear slope below γ_c (bounded, the small positive value a finite-window transient that depends on γ and N), a slope of 0.999—indistinguishable from unity—exactly at γ_c, and $\gtrsim 10$ above. Only the unit slope at γ_c is universal: the linear-in-t secular growth is the operational definition of the EP and the cleanest probe of the analyticity breakdown.

Analog realisation. In the sine basis the deformed operator is, exactly, a 1D non-Hermitian Wannier-Stark ladder—linear on-site energies $\pi g^2 N_c\, n$ (the confining spectrum) with imaginary nearest-neighbour hopping $-i\gamma/4$. Such ladders are engineered in photonic waveguide arrays (propagation distance $z \leftrightarrow t$, balanced gain/loss giving the imaginary hopping) [24], topolectrical RLC circuits (the admittance network is itself a continued fraction), and synthetic frequency dimensions; the Wannier-Stark/Bloch-oscillation regime was predicted by Longhi [25] and observed in PT-symmetric mesh [26] and silicon [27] photonic lattices (mappings in SM S3.2). Launching into the lowest mode and recording the output intensity (or voltage norm) reads off the three-regime law—accessible up to the tuning precision near γ_c and finite array size, with the EP cascade and skin effect of §5 on the same platforms, independent of any QCD realisation.

V. CONFINEMENT FINGERPRINTS AND THE NON-HERMITIAN SKIN EFFECT

Threshold locked to confinement. The exact linear scaling $\gamma_c = 7.966\, g^2N_c$ [Fig. 1(c)] shows that the imaginary coupling needed to break PT is set by the meson level spacing $\pi g^2 N_c$. Pushing γ further produces a regular cascade [Fig. 1(d)]: the k-th adjacent meson pair coalesces at $\gamma_c^{(k)} \simeq k\,\gamma_c^{(1)}$ (onsets $4.01, 8.14, 12.31$ at $g^2N_c = 0.5$, ratios $1 : 2.03 : 3.07$, N-independent)—the linearity is approximate, a first-order regularity of the equidistant ladder rather than an exact identity—with three levels never approaching, so the codimension forbids a higher-order EP with the single parameter γ. Both the threshold and the cascade spacing are spectroscopic

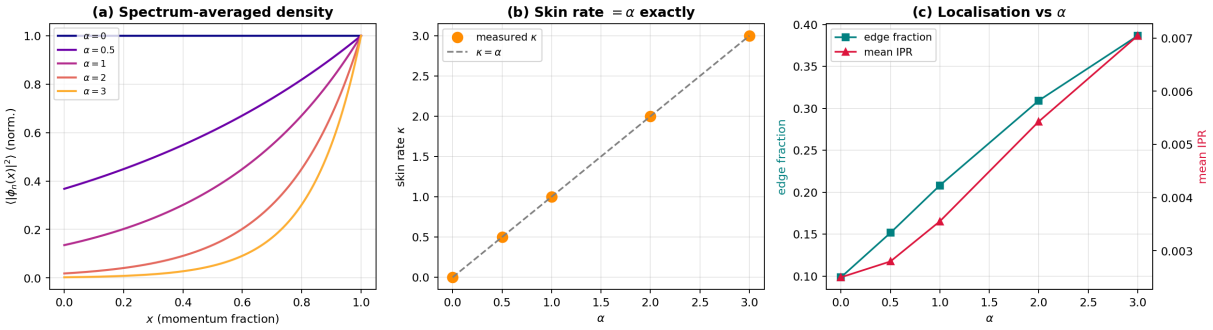

FIG. 3. NHSE from $V_\alpha = e^{\alpha X} V e^{-\alpha X}$ ($L = 600$, $g^2 N_c = 1$). (a) Spectrum-averaged density piles toward $x = 1$ as α grows. (b) Skin rate $\kappa = \alpha$ exactly (points on the dashed line). (c) Edge fraction and mean IPR grow with α, the spectrum staying real to 10^{-12}.

fingerprints of the equidistant, confining spectrum. (For $m > 0$ the EP shifts upward while $\nu = 1/2$ holds; see SM S6.1.)

Non-Hermitian skin effect. A second, independent deformation makes the gluon exchange non-reciprocal,

$$V_\alpha(x,y) = \mu^2 \frac{e^{\alpha(x-y)}}{(x-y)^2} = e^{\alpha x}\left[\mu^2 \frac{1}{(x-y)^2}\right] e^{-\alpha y}. \tag{7}$$

The factorisation makes $V_\alpha = e^{\alpha X} V e^{-\alpha X}$ an exact imaginary-gauge similarity transform of the Hermitian V. Hence the open-boundary (Dirichlet) spectrum is real and α-independent, and the right eigenvectors are $\phi_n^R(x) = e^{\alpha x}\phi_n(x)$—an exactly exponential skin of rate $\kappa = \alpha$. The momentum-fraction operator itself carries only Dirichlet ends; closing the corresponding level lattice into a ring—the geometry of the analog platforms above—makes the gauge factor $e^{\alpha x}$ multivalued, opening the spectrum into loops with winding $W = \mathrm{sgn}(\alpha)$ [28]. This point-gap topology places the model in the Hatano-Nelson universality class [9, 29]. Numerics confirm this to machine precision [Fig. 3, Table S2]: the spectrum stays real to within 10^{-12}, the measured skin rate equals α to three digits, and the boundary weight grows monotonically. This is worth contrasting with generic long-range nonreciprocity: power-law couplings $1/l^\beta$ make the skin *anomalous*—scale-free localisation with a system-size-dependent length and a real-to-complex spectral transition [36]—because a single imaginary-gauge transform Hermitises only the nearest-neighbour part and leaves the longer-range terms residually non-Hermitian. The 't Hooft kernel is special in a precise sense: its deformation $e^{\alpha(x-y)}$ is multiplicatively separable, so the *entire* hypersingular kernel is absorbed by the one similarity $e^{\alpha X}$ (Fig. S1). The non-locality is rendered inert not because long range is harmless in general, but because this particular nonreciprocity is gauge-compatible.

VI. DISCUSSION

The 't Hooft model's weighted Hermiticity provides an exactly-solvable baseline whose meson resolvent is a Herglotz J-fraction; deforming it exposes the breakdown of that analyticity at an exceptional point. The breakdown is fully characterised: its location is the continued-fraction root $\gamma_c = 7.966\, g^2 N_c$ (exactly 2π at the two-pole level), its order is $\nu = 1/2$ by the Jordan form, its dynamics is the linear secular growth of the propagator norm, and its threshold is locked to confinement and recurs as a uniform EP cascade. Mapping the model onto a non-Hermitian Wannier-Stark ladder makes all three signatures accessible in photonic and circuit analogues.

The deformation is the momentum-fraction analogue of the imaginary chemical potential of finite-density lattice QCD [7, 8], where γ_5-Hermiticity keeps the spectrum real until continuation fails at the Roberge-Weiss transition [30]; the 't Hooft EP is not a simulation of that mechanism (Roberge-Weiss needs compact links, Polyakov loops, centre symmetry, absent here) but shares, and renders solvable, its minimal structure. The same pattern underlies the Yang-Lee edge singularity [31]—a mechanistic analogy only, our EP being a spectral branch point ($\nu = 1/2$) rather than a non-unitary CFT critical point [32]. Relative to perturbative non-Hermitian gauge theories [13–17] and continuum NHSE [33, 34], the contribution is an exactly-solvable confining setting where the breakdown is located by a continued fraction, classified by a Jordan form, and probed by a secular law.

For an integrability-based approach to the 't Hooft spectrum at general quark mass, see Litvinov and Meshcheriakov [35]. We note that the continued-fraction formulation is exact at the chiral point and does not rely on additional conjectural relations.

We do not overstate scope: the lattice-QCD link is an analogy of mechanism, and the skin effect is the standard Hatano-Nelson class. A first-principles gauge derivation, an endpoint-adapted basis for the massive case, and entanglement dynamics across the breakdown are natural

next steps; beyond the classical analogues, dissipative cold-atom lattice-gauge simulators and driven-dissipative excitonic edges are further candidate platforms, each needing its own microscopic mapping.

This work was supported by the National High-Level Overseas Talent Program (KS21400126), the Suzhou Talent project (ZXP2025057), the Jiangsu Distinguished Professorship Fund (SR21400225), and the Research Start-up Fund (NH21400525).

[1] G. 't Hooft, "A Two-Dimensional Model for Mesons," *Nucl. Phys. B* **75**, 461 (1974).
[2] S. J. Brodsky, H.-C. Pauli, and S. S. Pinsky, "Quantum chromodynamics and other field theories on the light cone," *Phys. Rep.* **301**, 299 (1998).
[3] H. M. Nussenzveig, *Causality and Dispersion Relations* (Academic Press, New York, 1972).
[4] K. Liu, "Kramers-Kronig Relations and Causality in Non-Markovian Open Quantum Dynamics: Kernel, State, and Effective Kernel," arXiv:2604.17058 (2026).
[5] I. Rotter, "A non-Hermitian Hamilton operator and the physics of open quantum systems," *J. Phys. A: Math. Theor.* **42**, 153001 (2009).
[6] Y. Ashida, Z. Gong, and M. Ueda, "Non-Hermitian physics," *Adv. Phys.* **69**, 249 (2020).
[7] P. de Forcrand, "Simulating QCD at finite density," *PoS* **LAT2009**, 010 (2009).
[8] A. Roberge and N. Weiss, "Gauge theories with imaginary chemical potential and the phases of QCD," *Nucl. Phys. B* **275**, 734 (1986).
[9] N. Okuma, K. Kawabata, K. Shiozaki, and M. Sato, "Topological Origin of Non-Hermitian Skin Effects," *Phys. Rev. Lett.* **124**, 086801 (2020).
[10] W. D. Heiss, "The physics of exceptional points," *J. Phys. A: Math. Theor.* **45**, 444016 (2012).
[11] C. M. Bender and S. Boettcher, "Real Spectra in Non-Hermitian Hamiltonians Having PT Symmetry," *Phys. Rev. Lett.* **80**, 5243 (1998).
[12] K. Liu, "Topological Charge of Causality at a PT-Symmetric Exceptional Point," arXiv:2605.00117 (2026).
[13] M. C. Ogilvie and P. N. Meisinger, "PT Symmetry and QCD: Finite Temperature and Density," *SIGMA* **5**, 047 (2009).
[14] J. Alexandre, C. M. Bender, and P. Millington, "Non-Hermitian extension of gauge theories and implications for neutrino physics," *JHEP* **11**, 111 (2015).
[15] J. Alexandre, J. Ellis, P. Millington, and D. Seynaeve, "Gauge invariance and the Englert-Brout-Higgs mechanism in non-Hermitian field theories," *Phys. Rev. D* **99**, 075024 (2019).
[16] H. Raval and B. P. Mandal, "Deconfinement to confinement as PT phase transition," *Nucl. Phys. B* **946**, 114699 (2019).
[17] A. Fring and T. Taira, "Pseudo-Hermitian approach to Goldstone's theorem in non-Abelian non-Hermitian quantum field theories," *Phys. Rev. D* **101**, 045014 (2020).
[18] V. A. Fateev, V. A. Lukyanov, and A. B. Zamolodchikov, "On mass spectrum in 't Hooft's 2D model of mesons," *J. Phys. A: Math. Theor.* **42**, 304014 (2009).
[19] F. Ambrosino and S. Komatsu, "2d QCD and Integrability, Part I: 't Hooft model," *JHEP* **02**, 126 (2025).
[20] A. Mostafazadeh, "Pseudo-Hermiticity versus PT symmetry," *J. Math. Phys.* **43**, 205 (2002).
[21] E. N. Bulgakov, I. Rotter, and A. F. Sadreev, "Phase rigidity and avoided level crossings in the complex energy plane," *Phys. Rev. E* **74**, 056204 (2006).
[22] T. Kato, *Perturbation Theory for Linear Operators* (Springer, Berlin, 1966), Chap. II.
[23] H. S. Wall, *Analytic Theory of Continued Fractions* (Van Nostrand, New York, 1948).
[24] A. Regensburger, C. Bersch, M.-A. Miri, G. Onishchukov, D. N. Christodoulides, and U. Peschel, "Parity-time synthetic photonic lattices," *Nature* **488**, 167 (2012).
[25] S. Longhi, "Bloch Oscillations in Complex Crystals with PT Symmetry," *Phys. Rev. Lett.* **103**, 123601 (2009).
[26] M. Wimmer, M.-A. Miri, D. N. Christodoulides, and U. Peschel, "Observation of Bloch oscillations in complex PT-symmetric photonic lattices," *Sci. Rep.* **5**, 17760 (2015).
[27] Y.-L. Xu, W. S. Fegadolli, L. Gan, M.-H. Lu, X.-P. Liu, Z.-Y. Li, A. Scherer, and Y.-F. Chen, "Experimental realization of Bloch oscillations in a parity-time synthetic silicon photonic lattice," *Nat. Commun.* **7**, 11319 (2016).
[28] S. Yao and Z. Wang, "Edge States and Topological Invariants of Non-Hermitian Systems," *Phys. Rev. Lett.* **121**, 086803 (2018).
[29] N. Hatano and D. R. Nelson, "Localization Transitions in Non-Hermitian Quantum Mechanics," *Phys. Rev. Lett.* **77**, 570 (1996).
[30] M. D'Elia and M.-P. Lombardo, "Finite density QCD via imaginary chemical potential," *Phys. Rev. D* **67**, 014505 (2003).
[31] J. L. Cardy, "Conformal invariance and the Yang-Lee edge singularity in two dimensions," *Phys. Rev. Lett.* **54**, 1354 (1985).
[32] J. Lou, C. Chen, and Y. Wang, "Yang-Lee string-net model and η-self-adjoint Hamiltonians," *Phys. Rev. B* **108**, 115135 (2023).
[33] Y.-M. Hu, Y.-Q. Huang, W.-T. Xue, and Z. Wang, "Non-Bloch band theory for non-Hermitian continuum systems," *Phys. Rev. B* **110**, 205429 (2024).
[34] S. Longhi and G. Della Valle, "Non-Hermitian skin effect beyond the tight-binding models," *Phys. Rev. B* **105**, 165130 (2022).
[35] A. Litvinov and P. Meshcheriakov, "Meson mass spectrum in QCD_2 't Hooft's model," *Nucl. Phys. B* **1010**, 116766 (2025).
[36] Y.-C. Wang, H. H. Jen, and J.-S. You, "Scaling laws for non-Hermitian skin effect with long-range couplings," *Phys. Rev. B* **108**, 085418 (2023).
[37] Eqs. (DD-integral-prod) and (DD-integral-dev) of [35], derived from the resolvent representation of the 't Hooft equation.

VII. SUPPLEMENTAL MATERIAL — *EXCEPTIONAL POINTS AS ANALYTICITY BREAKDOWN IN THE 'T HOOFT MODEL*

Kejun Liu

This Supplement provides (S1) the functional-analytic setting of the 't Hooft operator and its weighted Hermiticity; (S2) the Jacobi continued-fraction (J-fraction) derivation of the EP threshold γ_c, including the closed-form two-pole value $2\pi g^2 N_c$ and the convergence to $7.966\, g^2 N_c$; (S3) the Jordan secular law for the propagator norm and the explicit mapping to non-Hermitian Wannier-Stark analog platforms; (S4) the exact imaginary-gauge similarity derivation of the skin effect, with numerical demonstration that the envelope is $e^{\alpha x}$; (S5) extended connections to Yang-Lee, Roberge-Weiss, and prior non-Hermitian gauge theory; (S6) technical notes on the massive case; and (S7) numerical tables. Equation/reference numbers refer to the main text unless prefixed "S".

A. Functional-analytic setting

1. The kernel and its domain

The 't Hooft operator is defined by the hypersingular principal-value integral

$$(V\phi)(x) = \mu^2\, P\!\int_0^1 \frac{\phi(y)}{(x-y)^2}\, dy, \qquad \mu^2 = g^2 N_c/\pi.$$

The kernel $(x-y)^{-2}$ is not Lebesgue-integrable, and the principal value is understood in the Hadamard finite-part sense, equivalent for our purposes to the subtracted form

$$(V\phi)(x) = \mu^2\, P\!\int_0^1 \frac{\phi(y)-\phi(x)}{(x-y)^2}\, dy \;-\; \mu^2\, \frac{\phi(x)}{x(1-x)},$$

using $P\!\int_0^1 (x-y)^{-2} dy = -1/[x(1-x)]$. For a general $\phi \in C^{0,\beta}$ the subtracted integrand behaves as $|x-y|^{\beta-2}$ near $y=x$, integrable only for $\beta > 1$; for the endpoint behaviour $\phi \sim \sqrt{x(1-x)}$ relevant here, convergence of the finite-part integral is secured by the specific 't Hooft kernel structure (the classical result), not by Hölder continuity alone.

We take the operator domain

$$D(V) = \{\phi \in L^2(0,1) :\ \phi(0) = \phi(1) = 0,\ \phi(x) \sim \sqrt{x(1-x)} \text{ at the endpoints},\ V\phi \in L^2_J\},$$

i.e. functions vanishing at the endpoints with the chiral-limit endpoint behaviour $\phi \sim \sqrt{x(1-x)}$ (the weight of the Gegenbauer parameter $\lambda = 1$ system; the endpoint exponent is $1/2$, not to be confused with λ). On this domain the subtracted integral converges and V maps into the weighted space $L^2_J \equiv L^2((0,1); [x(1-x)]^{-1/2} dx)$.

2. Weighted self-adjointness and reality of the spectrum

With the weighted inner product $\langle \phi, \psi \rangle_J = \int_0^1 \phi\bar{\psi}\, [x(1-x)]^{-1/2} dx$, integration by parts of the subtracted kernel (the boundary terms vanish because $\phi \sim \sqrt{x(1-x)}$) gives

$$\langle V\phi, \psi \rangle_J = \langle \phi, V\psi \rangle_J, \qquad \phi, \psi \in D(V),$$

so V is J-symmetric. Symmetry alone does not guarantee a real spectrum for an unbounded operator; one needs self-adjointness. Here this is supplied constructively: the change of variable $x = \sin^2(\theta/2)$ maps L^2_J isometrically onto $L^2(0,\pi)$ and carries V to an operator diagonalised by $\{\sin n\theta\}_{n\geq 1}$, the Gegenbauer system $\phi_n(x) = \frac{2\sqrt{2}}{\sqrt{\pi}} \sqrt{x(1-x)}\, C^{(1)}_{n-1}(2x-1)$. This system is complete in L^2_J (the sine functions $\{\sin n\theta\}$ are a complete orthonormal basis of $L^2(0,\pi)$, carried to L^2_J by the isometry), the eigenvalues $M_n^2 = \pi g^2 N_c\, n$ are real and simple, and V is therefore essentially self-adjoint on $D(V)$ with this complete orthonormal eigenbasis. The deficiency indices are $(0,0)$: the singular endpoints are in the limit-point case for the $\sqrt{x(1-x)}$ boundary behaviour, so no additional boundary conditions are required.

Two cautions, stated explicitly because they are easy to overstate:

1. **Hermiticity gives reality, not positivity.** A J-self-adjoint operator has a real spectrum; positivity $M_n^2 > 0$ is a separate, model-specific fact, here read off from the exact solution $M_n^2 = \pi g^2 N_c\, n$.
2. J **is unbounded.** The metric $J(x) = [x(1-x)]^{-1/2}$ diverges at the endpoints, so $(L^2, \langle\cdot,\cdot\rangle_J)$ is the completion L^2_J, not all of flat L^2. Because $J > 0$ on $(0,1)$ this is a genuine (positive-definite) Hilbert space, not a Krein space; the standard bounded-metric pseudo-Hermiticity theorems are not invoked, and are not needed, since self-adjointness is established directly from the eigenbasis.

3. *S1.3 The* PT *deformation*

The deformation $W(x) = i\gamma(x - 1/2) = -\frac{i\gamma}{2}\cos\theta$ is a *bounded* multiplication operator, so $V(\gamma) = V + W$ has the same domain $D(V)$ and is closed; relative boundedness of W with respect to V is trivial ($\|W\phi\| \le \frac{\gamma}{2}\|\phi\|$). The family $\gamma \mapsto V(\gamma)$ is therefore a holomorphic family of type (A) in Kato's sense [22], which justifies the Puiseux (square-root) expansion at the exceptional point used in the main text. The matrix elements in the sine basis are exactly tridiagonal,

$$\langle \sin m\theta | W | \sin n\theta \rangle = -\tfrac{i\gamma}{2} \cdot \tfrac{1}{2}(\delta_{m,n+1} + \delta_{m,n-1}),$$

so no quadrature is involved in the EP computations.

B. Jacobi continued-fraction derivation of the threshold

1. *The pencil is a Jacobi matrix*

In the sine basis $\{\sin n\theta\}$ the unperturbed operator is diagonal, $a_n = \langle n|V|n\rangle = \pi g^2 N_c\, n$, and the PT deformation $i\gamma(x-1/2) = -\frac{i\gamma}{2}\cos\theta$ is tridiagonal with off-diagonal $b = -i\gamma/4$ (from $\langle \sin m\theta|\cos\theta|\sin n\theta\rangle = \frac{1}{2}\delta_{|m-n|,1}$). Thus $V(\gamma)$ is a (complex, symmetric) Jacobi matrix, and the resolvent matrix element $G(z;\gamma) = \langle 1|(z - V(\gamma))^{-1}|1\rangle$ has the J-fraction form (4) with constant off-diagonal $b_n = -i\gamma/4$. At $\gamma = 0$ the spectral measure is positive and G is genuinely Herglotz/Nevanlinna; for $\gamma \neq 0$ the off-diagonals are imaginary, $b_n^2 = -\gamma^2/16 < 0$, so the classical Stieltjes positivity ($b_n^2 > 0$) is lost and (4) is a complex Jacobi continued fraction—the analytic continuation in γ of the Herglotz fraction. Its convergence is not covered by the positive-measure theorems; here it is established empirically (the threshold is stable from depth $K = 5$ through $K = 256$, §S2.4), consistent with the boundedness of the constant-b_n recurrence.

2. *Two-pole closed form*

The leading approximant retains the lowest two mesons,

$$V^{(2)}(\gamma) = \begin{pmatrix} \pi g^2 N_c & -i\gamma/4 \\ -i\gamma/4 & 2\pi g^2 N_c \end{pmatrix}, \qquad M_\pm^2 = \tfrac{3}{2}\pi g^2 N_c \pm \sqrt{\left(\tfrac{\pi g^2 N_c}{2}\right)^2 - \left(\tfrac{\gamma}{4}\right)^2}.$$

The discriminant vanishes (the two poles of G collide into a branch point) at

$$\boxed{\gamma_c^{(2)} = 2\pi g^2 N_c} \qquad (\approx 6.283\, g^2 N_c),$$

an exact closed form. Above it the pair is complex-conjugate, $M_\pm^2 = \frac{3}{2}\pi g^2 N_c \pm \frac{i}{4}\sqrt{\gamma^2 - (2\pi g^2 N_c)^2}$, giving the square-root branch (3) with $\nu = 1/2$ manifest.

3. *S2.3 The $K = 3$ truncation is a third-order point*

The next convergent is not a refined order-2 collision but, accidentally, an order-3 one. With $\Delta = \pi g^2 N_c$ and $b = -i\gamma/4$ the 3×3 Jacobi block has the exact factorisation

$$\det(J^{(3)} - zI) = (2\Delta - z)\left[(\Delta - z)(3\Delta - z) + \tfrac{\gamma^2}{8}\right],$$

so the central level $z = 2\Delta$ is an eigenvalue for *all* γ—a consequence of the reflection symmetry $a_n \leftrightarrow a_{N+1-n}$ of the equidistant ladder, which pins the centre of any odd, symmetric truncation. The remaining pair $z = 2\Delta \pm \sqrt{\Delta^2 - \gamma^2/8}$ meets the pinned centre when $\gamma^2 = 8\Delta^2$, i.e.

$$\gamma_c^{(3)} = 2\sqrt{2}\,\pi g^2 N_c \approx 8.886\, g^2 N_c,$$

where $\det(J^{(3)} - zI) = -(z - 2\Delta)^3$: algebraic multiplicity 3, geometric multiplicity 1 (the rank of $J^{(3)} - 2\Delta I$ is 2), a genuine third-order EP. This is a finite-truncation artefact: it requires the simultaneous, symmetric approach of *three* levels, available only because $N = 3$ is odd and small. Even truncations ($K = 4$) have no pinned centre, and the first onset reverts to the order-2 lowest-pair coalescence (numerically $\gamma_c^{(4)} = 7.948\, g^2 N_c$, with $\nu = 1/2$); larger K converge to the physical threshold. The overshoot of $\gamma_c^{(3)}$ in the convergence sequence is exactly this pinning—the third level must be dragged in—not a defect of the resolvent.

4. *Convergence of the full fraction*

Retaining K poles (depth-K J-fraction) and solving the coalescence condition gives a numerically convergent sequence for the true threshold (computed as the onset of complex eigenvalues; $g^2 N_c = 1$):

K	2	3	4	5	8	16	256
$\gamma_c(K)$	6.283	8.886	7.948	7.967	7.966	7.966	7.966

The sequence saturates to four digits by depth $K = 5$ and is stable through $K = 256$: the EP is controlled by the lowest five rungs of the continued fraction. The $\sim 27\%$ shift from the two-pole value 2π is the true contribution of the higher mesons (the deeper b_n rungs), not a truncation artifact—the threshold is analytic, $\gamma_c = 7.966\, g^2 N_c$, with $\gamma_c/(\pi g^2 N_c) = 2.536$. This is the analytic resolution of Fig. 2(a).

C. Jordan secular law and analog realisation

1. *Linear secular growth at the EP*

For $\gamma < \gamma_c$ the spectrum is real and $V(\gamma)$ is diagonalisable, $V = S\Lambda S^{-1}$, so $\|e^{-iVt}\| \le \kappa(S)$ is bounded in t (the constant is the eigenvector condition number / Petermann factor). Equivalently, in the PT-unbroken phase there is a positive metric $\eta(\gamma) = (SS^\dagger)^{-1}$ rendering $V(\gamma)$ η-self-adjoint; the bound is the condition number of η. It is finite for each fixed $\gamma < \gamma_c$ but *not uniform*: as $\gamma \to \gamma_c^-$ the eigenvectors align, η degenerates and $\kappa(S) \to \infty$. Consequently a finite-time log-log fit below γ_c returns a small, non-universal positive slope (a transient set by $\kappa(S)$ and the window), which should not be read as genuine power-law growth—the asymptotics are bounded; only the unit slope exactly at γ_c is universal. At $\gamma = \gamma_c$ the coalescing pair forms a 2×2 Jordan block $J = E_* I + \mathcal{N}$, $\mathcal{N}^2 = 0$; since $e^{-iJt} = e^{-iE_* t}(I - i\mathcal{N}t)$, the propagator acquires a term linear in t and

$$\left\|e^{-iV(\gamma_c)t}\right\| = \mathcal{O}(t) \qquad (t \to \infty).$$

For $\gamma > \gamma_c$ the complex pair gives $\|e^{-iVt}\| \sim e^{\Gamma t}$ with $\Gamma = \max \mathrm{Im}\, M^2 \propto \sqrt{\gamma - \gamma_c}$. A log–log fit of the computed norm over $t \in [4, 64]$ ($N = 160$) gives slopes 0.25 ($\gamma < \gamma_c$, bounded), 0.999 ($\gamma = \gamma_c$, linear), and $\gtrsim 10$ ($\gamma > \gamma_c$, exponential) [Fig. 2(b)]. The exactly-linear secular growth is the operational, phase-convention-free signature of the EP.

2. *Mapping to a non-Hermitian Wannier-Stark ladder*

The matrix $V(\gamma)$—on-site energies $a_n = \pi g^2 N_c\, n$ (a linear Stark gradient) with imaginary nearest-neighbour hopping $-i\gamma/4$—is a 1D non-Hermitian Wannier-Stark ladder. Concrete analog mappings:

- **Photonic waveguide array.** Waveguides $\leftrightarrow$ modes n; paraxial propagation distance $z \leftrightarrow$ time t; a linear refractive-index gradient realises a_n (Bloch oscillations); alternating gain (e.g. Er-doped, pumped) and loss synthesise the imaginary hopping. Total output intensity vs z reads off $\|e^{-iVt}\|$.

- **Topolectrical RLC circuit.** Nodes ↔ modes; Kirchhoff's laws map to the eigenproblem; graded grounding LC realises a_n; negative-impedance converters / op-amps supply non-reciprocal (imaginary) couplings. The admittance is itself a continued fraction, so γ_c appears as an impedance resonance—directly testing §S2.
- **Synthetic frequency dimension.** Frequency modes of a single ring resonator ↔ the level lattice; an electro-optic modulator imprints the imaginary inter-mode hopping.

In each, the three-regime growth law of §S3.1 (bounded / linear / exponential) is measured directly, making the analyticity breakdown an observable phenomenon independent of any QCD realisation.

D. The non-reciprocal kernel as an imaginary-gauge similarity

1. *Exact operator identity*

The non-reciprocal kernel factorises exactly,

$$V_\alpha(x,y) = \mu^2 \frac{e^{\alpha(x-y)}}{(x-y)^2} = e^{\alpha x}\Big[\mu^2 \frac{1}{(x-y)^2}\Big] e^{-\alpha y},$$

which at the operator level is the similarity transform

$$\boxed{V_\alpha = e^{\alpha X}\, V\, e^{-\alpha X}}, \qquad (X\phi)(x) = x\,\phi(x).$$

Since X is multiplication by $x \in (0,1)$, $e^{\pm\alpha X}$ are bounded, invertible multiplication operators on L^2_J ($\|e^{\pm\alpha X}\| \le e^{|\alpha|}$) that preserve $D(V)$ (the factor $e^{\pm\alpha x}$ is smooth and non-zero on $[0,1]$, so the endpoint behaviour is unchanged); the identity is therefore a true similarity transform. Three consequences follow with no approximation:

1. **Real, α-independent OBC spectrum.** Similar operators are isospectral, so $\mathrm{spec}(V_\alpha) = \mathrm{spec}(V) = \{\pi g^2 N_c\, n\}$ for all α under open boundaries.
2. **Exact exponential skin.** If $V\phi_n = M_n^2\phi_n$ then $V_\alpha(e^{\alpha x}\phi_n) = M_n^2(e^{\alpha x}\phi_n)$, so the right eigenvectors are $\phi_n^R(x) = e^{\alpha x}\phi_n(x)$ and (from $V_\alpha^\dagger = e^{-\alpha X}Ve^{\alpha X}$) the left eigenvectors are $\phi_n^L(x) = e^{-\alpha x}\phi_n(x)$. Every state is exponentially localised with skin rate exactly $\kappa = \alpha$, right states accumulating at $x \to 1$, left states at $x \to 0$; the sign reverses with α.
3. **Point-gap topology.** Under the physical open (Dirichlet) boundaries the spectrum is real (point gap closed). Periodic boundary conditions are not native to the momentum-fraction operator; the point-gap statement refers to the discretised N-level lattice (the analog-platform geometry of main-text §4) closed into a ring, where the imaginary-gauge factor $e^{\alpha x}$ becomes multivalued, the similarity fails, the spectrum opens into complex loops, and the spectral winding number is $W = \mathrm{sgn}(\alpha)$. The OBC→PBC spectral collapse and non-zero W on this lattice are the defining signatures of the non-Hermitian skin effect, placing it in the Hatano-Nelson universality class.

2. *Numerical confirmation (Fig. S1)*

In the sine basis, $X = (I - C)/2$ with C the tridiagonal $\cos\theta$ matrix, and we form $V_\alpha = e^{\alpha X}\,\mathrm{diag}(\pi g^2 N_c\, n)\, e^{-\alpha X}$ by matrix exponential — no hypersingular quadrature. Figure S1(a) shows the ratio $|\psi_\alpha(x)|/|\psi_0(x)|$ for the ground state (which has no interior nodes, giving a clean ratio): it lies exactly on $e^{\alpha x}$ (dotted) for $\alpha = 0.5, 1, 2, 3$. Figure S1(b) confirms the spectrum stays real to $\sim 10^{-12}$ for all α, as required by isospectrality with the Hermitian V.

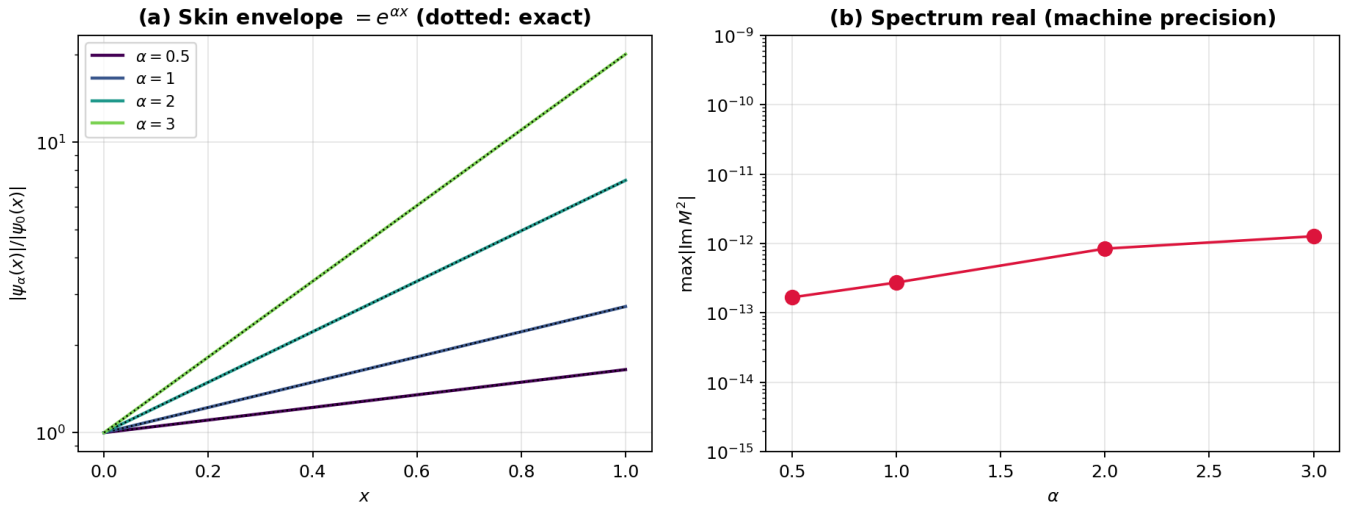

Figure S1. (a) Ground-state skin envelope $|\psi_\alpha(x)|/|\psi_0(x)|$ from $V_\alpha = e^{\alpha X} V e^{-\alpha X}$ ($L = 500$, $g^2 N_c = 1$); solid curves are numerical, dotted are $e^{\alpha x}$ — they coincide, confirming the skin rate is exactly α. (b) The largest $|\mathrm{Im}\, M^2|$ over the spectrum remains at the 10^{-12} level for all α, confirming the open-boundary spectrum is real (isospectral with V).

This settles a question raised in the main text: the long-range, hypersingular character of the 't Hooft kernel does not produce an anomalous (e.g. power-law) skin. The decay is exactly exponential, rate α, identical to the local Hatano-Nelson model — the non-locality is rendered inert by the gauge factorisation. The contrast with the generic long-range case is instructive. For nonreciprocal power-law couplings $1/l^\beta$ a single imaginary-gauge transform $\hat{c}_j \to e^{-gj}\hat{c}_j$ Hermitises only the nearest-neighbour ($l = 1$) hop; the longer-range terms pick up a mismatched factor $e^{\mp(l-1)g}/l^\beta$ and remain non-Hermitian, which is exactly what produces the scale-free localisation and the real-to-complex spectral transition reported by Wang, Jen, and You [36]. The 't Hooft deformation evades this because $e^{\alpha(x-y)} = e^{\alpha x} e^{-\alpha y}$ is multiplicatively separable across *all* distances, so the single similarity $e^{\alpha X}$ absorbs the whole kernel at once. The relevant dichotomy is therefore not short- versus long-range but gauge-incompatible versus gauge-compatible nonreciprocity.

E. Extended connections

1. *Yang-Lee edge singularity*

The Yang-Lee edge singularity (YLES) and our exceptional point share the qualitative pattern *imaginary coupling → real observables until a sharp threshold → complex thereafter*. They are not in the same universality class. The YLES is a thermodynamic singularity: zeros of the partition function in the complex fugacity (imaginary magnetic field) plane pinch the real axis only in the thermodynamic limit, the critical point being the non-unitary minimal CFT $\mathcal{M}_{2,5}$ ($c = -22/5$), with an edge exponent unrelated to $1/2$. Our EP is a spectral singularity of a single finite operator: eigenvalue and eigenvector coalescence with $\nu = 1/2$ fixed by the 2×2 Jordan normal form, present already at finite N and requiring no thermodynamic limit. The deformed 't Hooft model has no conformal symmetry and no RG flow to a Yang-Lee fixed point. Intrinsically non-Hermitian lattice realisations of Yang-Lee criticality (e.g. η-self-adjoint string-net models, Ref. [32]) carry a *fundamental* indefinite metric, the opposite of our positive-metric host whose non-Hermiticity is introduced only by deformation.

2. *Roberge-Weiss transition and the sign problem*

In lattice QCD at finite baryon density the fermion determinant $\det D(\mu_B)$ is complex for real μ_B (the sign problem). Simulating at imaginary $\mu_B = i\mu_I$ restores γ_5-Hermiticity and a real, positive determinant; observables are then analytically continued $\mu_I \to -i\mu_B$ (Refs. [7, 8]). This continuation is bounded by the Roberge-Weiss transition at $\mu_I = \pi T/3$ (Ref. [30]), a bona fide first-order thermodynamic transition driven by centre-symmetry breaking of the *compact* gauge group. None of the Roberge-Weiss ingredients — compact links, Polyakov loops, centre symmetry —

exist in the 1+1D large-N_c model in light-cone gauge $A^+ = 0$. The connection we draw is therefore strictly at the level of the shared *minimal* mechanism: an imaginary coupling that protects a real spectrum up to a sharp threshold beyond which analytic continuation diverges. The 't Hooft EP provides an exactly-solvable instance where the breakdown — the square-root branch point $\delta M^2 \propto \sqrt{\gamma_c - \gamma}$ — can be exhibited in closed analytic and high-precision numerical form. We make no claim of simulating finite-density QCD.

3. *Prior non-Hermitian gauge theory*

Non-Hermitian and PT-symmetric gauge theories have been studied by Raval and Mandal (deconfinement as a PT transition, Ref. [16]), Ogilvie and Meisinger (PT symmetry in QCD at finite T, μ, Ref. [13]), Alexandre–Bender–Millington and Alexandre–Ellis–Millington–Seynaeve (rigorous non-Hermitian gauge extensions and the Englert-Brout-Higgs mechanism, Refs. [14, 15]), and Fring and collaborators (non-Hermitian gauge field theory, BPS limits, EPs in 't Hooft-Polyakov monopole spectra, Ref. [17]). These are first-principles constructions of *intrinsically* non-Hermitian theories, predominantly perturbative. Our contribution is orthogonal: a *deformation* of the non-perturbatively confining, exactly-solvable 't Hooft model, which makes the EP exponent, the confinement-locked threshold $\gamma_c = 7.97\, g^2 N_c$, the EP cascade, and the NHSE all accessible against an analytically known $\gamma = 0$ baseline. Continuum NHSE is itself established (Refs. [33, 34]); the novelty here is its realisation in a confining gauge theory.

F. Technical notes

1. *Massive quarks and basis bias*

For $m_1, m_2 > 0$ the endpoint exponents β_i solve $\beta_i \pi \cot(\beta_i \pi) = 1 - m_i^2/\mu^2$ and are generically irrational. The sine basis is built for the chiral-limit $\sqrt{x(1-x)}$ endpoint behaviour; for $m > 0$ it is sub-optimal, and the finite-N EP exponent acquires a basis bias (we find $\nu_\infty \approx 0.514$ at $m = 0.1$ rather than 0.5). The exponent $\nu = 1/2$ is nonetheless guaranteed by the order-2 Jordan structure, independent of the mass. A basis adapted to the endpoint exponents (Jacobi polynomials $P_n^{(2\beta_1, 2\beta_2)}$) would remove the bias; the corresponding FSS for $m > 0$ is left to future work. At $g^2 N_c = 0.5$ (the convention of this subsection; the chiral value 3.98 is $7.97\, g^2 N_c$, consistent with §S2.4), the threshold trend $\gamma_c = 3.98\,(m{=}0) \to 4.26\,(m{=}0.1)$ — the mass stabilising the PT-unbroken phase — is robust.

2. *Propagator-norm computation*

The three-regime law of §S3.1 is computed from the operator 2-norm $\|e^{-iV(\gamma)t}\|_2$ (largest singular value), evaluated by dense `scipy.linalg.expm` at $N = 160$—robust even at the defective EP, unlike eigenvector-based reconstructions which are ill-conditioned there (Petermann blow-up). The single-state survival amplitude $\langle\phi_0|e^{-iVt}|\phi_0\rangle$ shows the same qualitative transition but is contaminated by Petermann factors; the propagator norm is the clean, basis-independent diagnostic. A quantitative biorthogonal treatment (entanglement dynamics across the (γ, α) plane) is left to future work.

3. *Test of the FLZ D-Q conjecture at the chiral point*

The FLZ integrability programme [18, 35] provides a complementary approach to the 't Hooft model through a Baxter TQ equation. Two routes exist from the Q-function to spectral data. The first is a pair of rigorous integral relations[37] expressing $\partial_\lambda \log D_\pm$ as integrals of $Q_\pm$ and their derivatives. These are exact but, as noted in [18, 35], computationally impractical—their evaluation becomes *"very cumbersome"* at higher orders, and one of them *"behaves badly"* at large λ. The second route is the D-Q relation—a much simpler local formula,

$$\partial_\lambda \log D_\pm(\lambda) = 2i\, \partial_\nu \log Q_\mp(\nu)\big|_{\nu=i},$$

which FLZ [18] *"guessed"* (their word) for $\alpha = 0$ as a shortcut replacing the intractable integrals. It was extended to $\alpha \neq 0$ in [35] (eq. (2.17-new)). Its status is explicitly noted as unproven in those works—FLZ wrote *"has not been proven rigorously"*, and Ref. [35] adds that all $s > 1$ spectral sums *"are of conjectural nature"* because they depend

on it. The chiral point $\alpha = -1$ is the unique parameter value where the meson spectrum is known in closed form, providing an exact benchmark against which this conjectural shortcut can be tested.

Spectral sums at the chiral point. At $\alpha = -1$ the spectrum is $\lambda_n = n/2$ ($n \geq 1$) with $\lambda_0 = 0$ (massless pion). The regularised odd spectral sums [18] are

$$G_-^{(1)} = \sum_{n=0}^{\infty} \Big(\frac{1}{\lambda_{2n+1}} - \frac{1}{n+1} \Big) = 2\log 2, \tag{8}$$

$$G_-^{(s)} = \sum_{n=0}^{\infty} \frac{1}{\lambda_{2n+1}^s} = 2^s(1 - \tfrac{1}{2^s})\zeta(s) \quad (s \geq 2). \tag{9}$$

Chiral-limit formulas from Paper 1. Reference [35] gives the $a \to 0$ expansion of $G_-^{(s)}$ at $\alpha = -1+a$ (eqs. (5.5)–(5.7)), e.g.

$$G_-^{(1)}(-1+a)\big|_{a\to 0} = \log(8\pi) - 3 - \frac{7\zeta(3)}{\pi^2} + \frac{1}{2}(c_1^{(0)} - c_3^{(0)}) + \mathcal{O}(\sqrt{a}), \tag{10}$$

$$G_-^{(2)}(-1+a)\big|_{a\to 0} = \frac{10}{3} + \frac{56\zeta(3)}{3\pi^2} - \frac{124\zeta(5)}{\pi^4} + 2(c_3^{(0)} - c_5^{(0)}) + \mathcal{O}(\sqrt{a}). \tag{11}$$

The coefficients $c_{2k-1}^{(0)}$ are the $O(1)$ terms in the chiral expansion of the integrals $u_{2k-1}(\alpha) = \int_{-\infty}^{\infty} \frac{\sinh^2 t}{t\cosh^{2k-1} t(\alpha \sinh t + t\cosh t)} dt$. As $\alpha \to -1$, a pole $t_1^* \approx i\sqrt{3a}$ approaches the real axis; Ref. [35] splits $u_{2k-1} = u_{2k-1}^{(1)} + u_{2k-1}^{(2)}$ into a residue part $u_{2k-1}^{(1)} = \sqrt{3}\pi/\sqrt{a} + \cdots$ and a regular part whose $a \to 0$ limit defines

$$c_{2k-1}^{(0)} \equiv \int_{-\infty+i\varepsilon}^{\infty+i\varepsilon} \frac{\sinh^2 t}{t\cosh^{2k-1} t\,(t\cosh t - \sinh t)}\, dt, \tag{12}$$

evaluated on a contour shifted above the real axis.

Method A: direct $u_1 - u_3$ from principal-value integrals. For $\alpha = -1+a$ with small $a > 0$, $u_1(\alpha)$ and $u_3(\alpha)$ are computed by principal-value quadrature to $\sim 10^{-10}$ accuracy. Both share the same leading residue $\sqrt{3}\pi/\sqrt{a}$, which cancels in the difference:

$$u_1 - u_3 = (c_1^{(0)} - c_3^{(0)}) + \mathcal{O}(\sqrt{a}).$$

Fitting $u_1 - u_3 = A + B\sqrt{a} + Ca$ over $a \in [10^{-5}, 10^{-2}]$ (15 points) gives $A = \mathbf{7.592}$.

Method B: contour integration of the defining integral. Equation (12) is evaluated directly by high-precision mpmath quadrature on the contour $\mathrm{Im}\, t = \varepsilon = 0.3$. The result is stable under variation of $\varepsilon \in [0.2, 0.5]$ (the $3/t^2$ leading singularity at $t = 0$ integrates to zero analytically on the shifted contour, so the finite part converges). We obtain

$$c_1^{(0)} = -4.184, \qquad c_3^{(0)} = -11.767, \qquad c_5^{(0)} = -15.928. \tag{13}$$

Hence $c_1^{(0)} - c_3^{(0)} = \mathbf{7.583}$ and $c_3^{(0)} - c_5^{(0)} = \mathbf{4.160}$.

Method C: direct evaluation of the spectral-sum formula. Reference [35] also gives $G_-^{(1)}$ directly in terms of u_1, u_3 (eq. (3.34)):

$$G_-^{(1)} = \log(8\pi) - 3 + \frac{7\alpha\zeta(3)}{\pi^2} - \frac{\alpha}{2}(u_1(\alpha) + \alpha u_3(\alpha)).$$

Evaluating the right-hand side at $\alpha = -1 + a$ ($a = 10^{-5}$ to 10^{-2}) gives $G_-^{(1)} \approx 3.0$–3.15, while the exact chiral-limit value is $2\log 2 \approx 1.386$.

Results. The three methods are collected in Table S3.

Methods A and B agree to within 0.1% on $c_1^{(0)} - c_3^{(0)}$, but the value differs from the D-Q prediction by a factor ~ 1.88. Consequently the chiral-limit spectral-sum formulas of [35] do not recover the exact $\alpha = -1$ spectral sums. The $1/\sqrt{a}$ divergences (from the pion pole in $u_{2k-1}^{(1)}$) are unaffected; the discrepancy resides entirely in the finite constant part.

We emphasise that this concerns only the D-Q relation—the conjectural shortcut (2.17-new) of [35]. The underlying rigorous integral relations connecting Q-functions to spectral determinants are unaffected; the TQ-equation derivation and the Q-function construction remain on solid ground. The Jacobi continued fraction used in the main text requires no such auxiliary conjecture: the coefficients $\{a_n, b_n\}$ are exact, the spectral determinant is $\lim_{N\to\infty} B_N(z)$, and the recurrence $B_{n+1} = (z - a_{n+1})B_n - b_n^2 B_{n-1}$ is the discrete analogue of the TQ equation.

TABLE I. D-Q conjecture test at the chiral point.

Quantity	Method A (PV diff.)	Method B (contour)	D-Q required	Exact
$c_1^{(0)} - c_3^{(0)}$	7.592	7.583	4.029	—
$c_3^{(0)} - c_5^{(0)}$	—	4.160	0.324	—
$G_-^{(1)}$ (from $c^{(0)}$)	3.168	3.163	—	1.386
$G_-^{(2)}$ (from $c^{(0)}$)	—	12.608	—	4.935

G. Numerical tables

Table S1 — FSS of the EP critical exponent $\nu(N)$ in the chiral limit ($m = 0$), $g^2 N_c = 1$. The series is coupling-independent (identical for $g^2 N_c = 0.5, 1, 2$ by scale invariance). A linear $1/N$ fit extrapolates to $\nu_\infty = 0.4993$; a quadratic $1/N^2$ fit, favoured by the curvature ($R^2 = 0.9996$), gives $\nu_\infty = 0.5000$, consistent with the analytic value.

L	N	ν	R^2
200	199	0.5045	0.9830
400	399	0.5012	0.9924
600	599	0.5006	0.9950
800	799	0.5004	0.9964
1000	999	0.5003	0.9971
1500	1499	0.5001	0.9981
2000	1999	0.5001	0.9986
∞	—	**0.4993**	—

Table S2 — NHSE diagnostics for $V_\alpha = e^{\alpha X} V e^{-\alpha X}$ ($L = 600$, $g^2 N_c = 1$). Skin rate κ = slope of $\ln|\phi_n^R(x)|$ vs x for a representative bulk state; edge fraction = mean right-eigenvector weight in $x \in [0.9, 1]$, averaged over the spectrum.

α	max|Im M^2|	skin rate κ	edge fraction	mean IPR
0.0	0	0.000	0.098	0.0025
0.5	3×10^{-13}	0.500	0.151	0.0028
1.0	7×10^{-13}	1.000	0.208	0.0036
2.0	2×10^{-12}	2.000	0.309	0.0054
3.0	2×10^{-12}	3.000	0.387	0.0070